JACS
JOURNAL OF THE AMERICAN CHEMICAL SOCIETY
Article
pubs.acs.org/JACS

Ti^{3+}-, $V^{2+/3+}$-, $Cr^{2+/3+}$-, Mn^{2+}-, and Fe^{2+}-Substituted MOF-5 and Redox Reactivity in Cr- and Fe-MOF-5

Carl K. Brozek and Mircea Dincă*

Department of Chemistry, Massachusetts Institute of Technology, 77 Massachusetts Avenue, Cambridge, Massachusetts 02139, United States

Supporting Information

ABSTRACT: The metal nodes in metal−organic frameworks (MOFs) are known to act as Lewis acid catalysts, but few reports have explored their ability to mediate reactions that require electron transfer. The unique chemical environments at the nodes should facilitate unusual redox chemistry, but the difficulty in synthesizing MOFs with metal ions in reduced oxidation states has precluded such studies. Herein, we demonstrate that $MZn_3O(O_2C-)_6$ clusters from Zn_4O(1,4-benzenedicarboxylate)$_3$ (MOF-5) serve as hosts for V^{2+} and Ti^{3+} ions and enable the synthesis of the first MOFs containing these reduced early metal ions, which can be accessed from MOF-5 by postsynthetic ion metathesis (PSIM). Additional MOF-5 analogues featuring Cr^{2+}, Cr^{3+}, Mn^{2+}, and Fe^{2+} at the metal nodes can be obtained by similar postsynthetic methods and are reported here for the first time. The inserted metal ions are coordinated within an unusual all-oxygen trigonal ligand field and are accessible to both inner- and outer-sphere oxidants: Cr^{2+}- converts into Cr^{3+}-substituted MOF-5, while Fe^{2+}-MOF-5 activates NO to produce an unusual Fe-nitrosyl complex.

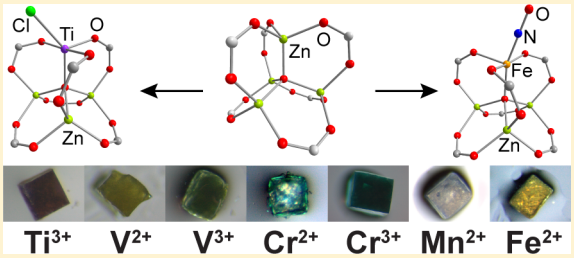

INTRODUCTION

The secondary building units (SBUs) in metal−organic frameworks (MOFs) can be regarded as electronically isolated molecular units that often lack structural precedent in molecular chemistry. Because of their site isolation, some SBUs feature metal cations with up to four open coordination sites,[1] priming them for inner-sphere redox reactivity. Despite these attractive properties, reactivity and catalysis studies of SBUs in MOFs have centered on their Lewis acid properties,[2] while studies of their *redox* reactivity remain an area open for exploration.[3−5] The dearth of SBU redox reactivity studies is partly due to the general incompatibility of reduced metal cations such as Ti^{3+}, V^{2+}, and Cr^{2+} with the typical conditions required for MOF synthesis, which often mediate the oxidation of such species. Among the thousands of reported MOFs, none are known to contain Ti^{3+} or V^{2+},[5−7] while those made from Cr^{2+} or Fe^{2+} are exceedingly rare.[4,8−12] Employing reactive cations to access SBUs without molecular precedent would pave the way to novel coordination chemistry and potentially to unprecedented redox catalysis.[13] Herein, we report that Ti^{3+}, V^{2+}, V^{3+}, Cr^{2+}, Cr^{3+}, Mn^{2+}, and Fe^{2+} incorporate into the SBUs of MOF-5 using mild synthetic methods. As shown below, the $MZn_3O(O_2C-)_6$ clusters in MOF-5 offer electronically unique and structurally flexible dianionic pseudotetrahedral or pseudotrigonal bipyramidal all-oxygen coordination environments. We demonstrate that MOF-5,[14] conveyed as a ligand, enables reactions of the inserted metal ions with both inner- and outer-sphere oxidants, which are requisites for small molecule activation. Thus, we provide the first evidence of redox activity in MOF-5 analogues with the stoichiometric single electron oxidation of Cr^{2+}-MOF-5, and demonstrate that Fe-MOF-5 activates NO via electron transfer from the Fe center.

RESULTS AND DISCUSSION

The redox-active MOF-5 analogues, denoted M-MOF-5 and ClM-MOF-5 for divalent and trivalent inserted metal ions, respectively, were accessed using postsynthetic ion metathesis (PSIM)[1,15−27] at room temperature under conditions mirroring those we reported for the isolation of Ni-MOF-5.[13] Although Ni-MOF-5 could be obtained by direct solvothermal synthesis from $Ni(NO_3)_2$ and $Zn(NO_3)_2$, attempts to synthesize (Cl)M-MOF-5 analogues directly by reacting terephthalic acid with $Zn(NO_3)_2$ and Ti^{3+}, $V^{2+/3+}$, Cr^{2+}, Mn^{2+}, or Fe^{2+} salts were unsuccessful. Instead, soaking crystals of MOF-5 in concentrated DMF solutions of VCl_2(pyridine)$_4$, $CrCl_2$, $MnCl_2$, and $Fe(BF_4)_2{\cdot}6H_2O$ for one week furnished M-MOF-5 (M = V^{2+}, Cr^{2+}, Mn^{2+}, or Fe^{2+}), while identical procedures involving $TiCl_3{\cdot}3THF$, $VCl_3{\cdot}3THF$, or $CrCl_3{\cdot}3THF$ produced ClM-MOF-5 (M = Ti^{3+}, V^{3+}, or Cr^{3+}) (Figure 1). Powder X-ray diffraction patterns of the (Cl)M-MOF-5 materials, shown in Figure 2, confirmed that the materials retained the MOF-5 morphology. Discrepancies in peak intensities are due to preferential orientation because we avoided grinding the samples in order to preserve their structural integrity. Although additional peaks were observed for Cr-MOF-5 and ClV-MOF-5 at 2θ = 7.0° and 13°, potentially indicative of long-range order

Received: June 28, 2013
Published: July 31, 2013

   dx.doi.org/10.1021/ja4064475 | J. Am. Chem. Soc. 2013, 135, 12886−12891

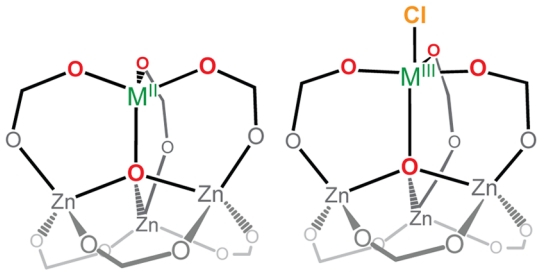

Figure 1. MOF-5 cluster acts as a unique tripodal chelating ligand for pseudotetrahedral V^{2+}, Cr^{2+}, Mn^{2+}, Fe^{2+}, Co^{2+}, and Ni^{2+} and pseudotrigonal bipyramidal Ti^{3+}, V^{3+}, and Cr^{3+} with terminal chloride moieties. These molecular structures depict substitution of a single Zn atom, although higher degrees of substitution are possible (see Table 1).

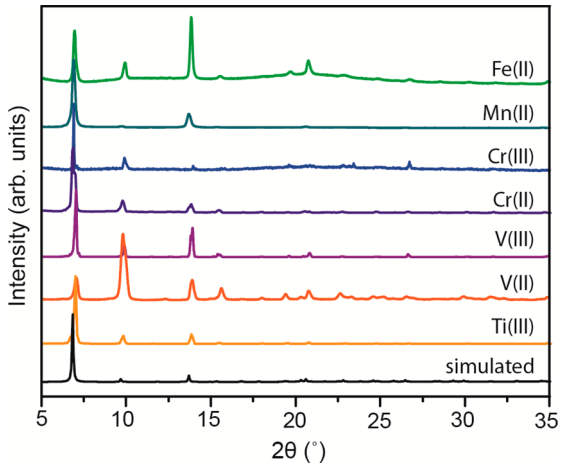

Figure 2. Powder X-ray diffraction patterns of MOF-5 exchanged with Ti^{3+}, V^{3+}, V^{2+}, Cr^{3+}, Cr^{2+}, Mn^{2+}, and Fe^{2+} juxtaposed with the calculated pattern of MOF-5.

imposed by the inserted metal ions, a supercell was not discernible by single crystal X-ray diffraction.[28]

We determined the degree of cation substitution and the formula of each new MOF-5 analogue by inductively coupled atomic emission spectroscopy (ICP-AES) and elemental microanalysis (EA). As shown in Table 1, the degree of

Table 1. Molecular Formulas of (Cl)M-MOF-5 Based on ICP-AES Results and C, H, N, Cl Elemental Analysis

(Cl)M-MOF-5	molecular formula
ClTi-MOF-5	$Zn_{3.91}Ti_{0.09}Cl_{0.09}O_{13}C_{24}H_{12}\cdot(DCM)$
V-MOF-5	$Zn_{3.83}V_{0.17}O_{13}C_{24}H_{12}$
ClV-MOF-5	$Zn_{3.80}V_{0.20}Cl_{0.20}O_{13}C_{24}H_{12}$
Cr-MOF-5	$Zn_{3.06}Cr_{0.94}O_{13}C_{24}H_{12}$
ClCr-MOF-5	$Zn_{2.59}Cr_{1.41}Cl_{1.41}O_{13}C_{24}H_{12}\cdot(DMF)_{0.4}$
Mn-MOF-5	$Zn_{3.58}Mn_{0.42}O_{13}C_{24}H_{12}$
Fe-MOF-5	$Zn_{3.04}Fe_{0.96}O_{13}C_{24}H_{12}$

exchange after 1 week under otherwise identical conditions varied drastically. Because the rate of solvent and ligand exchange depends on the nature of each cation, this data suggests that the ion metathesis reactions do not reach equilibrium after 1 week. Instead, the degree of exchange is kinetically controlled by the stability constants of each substituting cation.[29] The agreement between ICP-AES metals analysis and the C, H, and N analysis by EA confirms that the cations exchanged into the Zn_4O clusters and did not simply reside in the pores. Furthermore, we did not find evidence of halides or other anions that would necessarily be included for charge balance if metal addition, rather than substitution, occurred. These results are consistent with the structural assignment in Ni-MOF-5 and Co-MOF-5 where definitive substitution into the SBUs had been demonstrated previously.[13,30,31] Energy-dispersive X-ray (EDX) spectra and optical microscope images of these samples depict the inserted metal ions distributed throughout the crystals, not solely at the surface (see Figures S1–S7 in the Supporting Information), demonstrating that homogeneous substitution occurs throughout the entire crystal.[32] Moreover, because the shape of the crystals and the total crystalline mass did not change throughout the PSIM procedure, these data suggest that the substitution occurs in a crystal-to-crystal fashion rather than a dissolution–recrystallization mechanism.

Electronic spectroscopy provided additional evidence for the formation of site-isolated $(Cl)_xM_xZn_{4-x}O(O_2C-)_6$ clusters. A diffuse reflectance UV–vis–NIR spectrum of activated ClTi-MOF-5 showed absorption bands in the visible region at 450 and 625 nm, which our time-dependent DFT (TD-DFT) suggest are predominately d → π* (aryl) transitions. Although these charge transfer bands also overlap with lower intensity spin-forbidden d → d transitions, predicted by TD-DFT in the same region, transitions involving d electrons are consistent with a Ti^{3+} oxidation state. The high Cr loading in Cr-MOF-5 and ClCr-MOF-5 enabled sufficient absorbance in the UV–vis–NIR region to permit well-resolved diffuse reflectance spectra, shown in Figure 3. These differ from the absorption

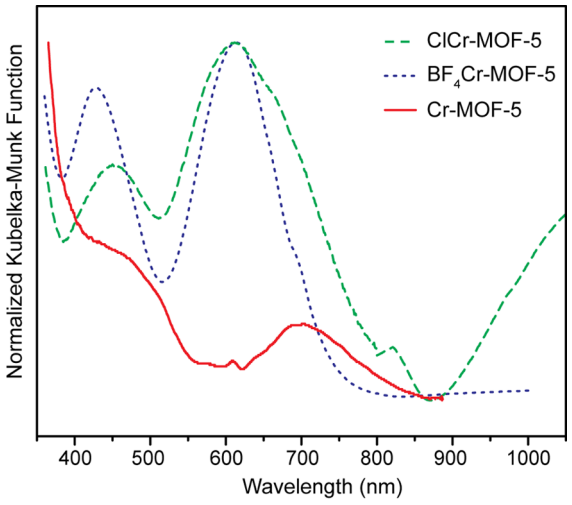

Figure 3. Diffuse reflectance UV–vis–NIR spectra of ClCr-MOF-5, Cr-MOF-5, and Cr-MOF-5 after treatment with $NOBF_4$ to afford BF_4Cr-MOF-5.

profiles of the starting materials, $CrCl_2$ and $CrCl_3\cdot3THF$ in DMF, with absorption maxima that are shifted to higher energy, as expected for the stronger ligand field provided by MOF-5.[13] The spectra of these materials would show additional overlapping absorptions bands if other metal complexes resided in the pores; the lack of such electronic absorption features further supports the assertion that substitution occurs at the metal nodes.

dx.doi.org/10.1021/ja4064475 | J. Am. Chem. Soc. 2013, 135, 12886–12891

Electron paramagnetic resonance (EPR) spectroscopy provided further confirmation of the oxidation state, coordination environment, and the associated electronic structures of the inserted metal ions. Indeed, materials with half-integer spin cations, expected to display degenerate ground m_s states (Kramers doublet ions), produced spectra that differed from the parent solutions. Thus, ClTi-MOF-5 displayed a well-resolved, sharp axial signal consistent with an $S = {}^1/_2$ system with $g_{x,y} = 1.93$ and $g_z = 2.09$ (Figure S10 in the Supporting Information), while Mn-MOF-5 and ClCr-MOF-5 produced broad axial signals (see Figures S8 and S9). As expected for an $S = {}^5/_2$ ($L = 0$) ion, the broad signal of Mn-MOF-5 fits to $g_{iso} = 2.00$, while the spectrum of ClCr-MOF-5 illustrates the strong axial symmetry imparted by the terminal chloride on the $S = {}^3/_2$ ion, giving $g_z = 4.27$ and $g_{x,y} = 1.93$. We assign the difference in resolution between the Ti^{3+}- and Cr^{3+}/Mn^{2+}-MOF-5 to the higher Cr and Mn content relative to Ti. Because the inserted metal ions incorporate homogeneously throughout the lattice, as discussed above, higher loadings bring the paramagnetic ions in close proximity, leading to short spin−spin relaxation times and loss of signal and hyperfine resolution in the Cr and Mn materials.[33] The signals for these two MOFs are nevertheless consistent with Mn^{2+} and Cr^{3+} trapped in solid lattices (see Figures S8 and S9 in the Supporting Information).[34,35] Our explanation for the resolution differences in the EPR spectra is corroborated by the spectrum collected for V-MOF-5, shown in Figure 4, where the low loading of the $I = {}^7/_2$ ^{51}V nucleus (see Table 1) enabled the resolution of fine structure and permitted a quantitative analysis of the axial symmetry and metal−ligand interaction. Here, the curvature of the baseline is likely a broad signal resulting from V^{2+} ($S = {}^3/_2$) ions that are in near proximity, making the overall signal a superposition of short and long T_2 values. A good fit to the spectrum of V-MOF-5 was obtained using $g_{x,y} = 1.97$, $g_z = 1.93$, $A_{x,y} = -200.66$ MHz, $A_z = -539.72$ MHz, and $S = {}^3/_2$. The strong axial signal is consistent with the expected C_{3v} symmetry about V^{2+}, while the large difference in the hyperfine coupling constants reveals the dissimilarity between the metal-μ_4-oxo bond and that with the carboxylate oxygen atoms. Fe-MOF-5, Cr-MOF-5, and ClV-MOF-5, all expected to be of integer spin, were indeed EPR silent.

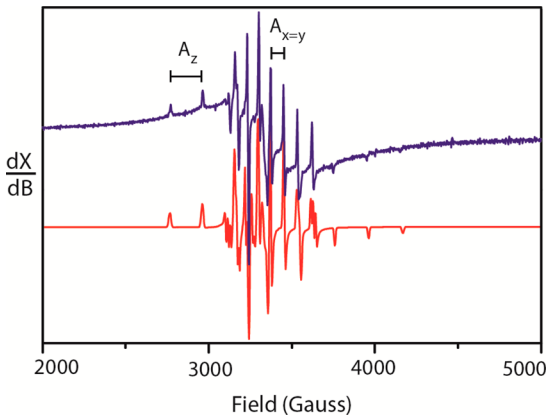

Figure 4. Continuous wave X-band EPR spectrum of V-MOF-5 at 77 K (blue) and a simulated trace (red).

To examine the porosity of the MOF-5 analogues, the materials were activated under conditions reported for pristine MOF-5.[36] N_2 adsorption isotherms collected at 77 K (see Figure S11 in the Supporting Information) confirmed that all the materials were highly porous, with apparent BET surface areas ranging from 2393 m^2/g for V-MOF-5 to 2700 m^2/g for ClCr-MOF-5. These are lower than the highest value reported for MOF-5, 3300 m^2/g,[36] and that reported for Ni-MOF-5.[13] We note, however, that the exchange of Ni^{2+} is much slower than those observed with the cations we report here; the rapid exchange of these metals might partially disrupt the MOF lattice and introduce defects that lead to reduced surface areas. We are currently studying the PSIM mechanism and the degree of disorder introduced during these exchanges.

Our motivation for incorporating metal ions with reduced oxidation states in MOF-5 was to enable redox reactivity at the SBUs. To demonstrate the viability of this strategy, we monitored the response of representative examples of these to both inner- and outer-sphere oxidants. Thus, combining green crystals of Cr^{2+}-MOF-5 with $NOBF_4$ in acetonitrile caused the rapid formation of blue $(BF_4)Cr^{3+}$-MOF-5. The transformation from Cr^{2+} to Cr^{3+} within MOF-5 was examined by electronic spectroscopy of activated samples, shown in Figure 3. Similar to ClTi-MOF-5, the λ_{max} at 700 nm of the Cr^{2+} material arises from a d → π* (aryl) transition, while both Cr^{3+} materials exhibit λ_{max} at 620 nm, assignable to d → d transitions. The small blue-shift of the higher energy peak in (BF_4)Cr-MOF-5 versus ClCr-MOF-5 can be attributed to the different geometries of the pseudotetrahedral Cr^{3+} center in the former versus that of the Cr^{3+} ion in the latter. TD-DFT calculations of geometry-optimized truncated models of the $Cr^{3+}Zn_3O(O_2C-)_6$ SBUs with and without coordinated chloride anions agree well with the experimental traces for the Cr^{3+}-substituted MOF-5 analogues and therefore substantiate a single electron oxidation of Cr^{2+} to Cr^{3+} (see Figures S13−S16 in the Supporting Information). PXRD and N_2 isotherms of (BF_4)Cr-MOF-5 confirm that the lattice remains crystalline and porous after the oxidation reaction (see Figures S17 and S18 in the Supporting Information). Though the overall N_2 uptake decreases to give a surface area of 1010 $m^2 g^{-1}$, the initial uptake of (BF_4)Cr-MOF-5 at low pressures mirrors what is normally observed for MOF-5, while the second expected uptake does not occur at higher pressures (as shown in the inset of Figure S18). Following a report by Snurr et al.,[37] this initial uptake corresponds to N_2 covering the pore exterior, while the absence of the second suggests the pore interiors may be blocked by solvated BF_4^- ions.

We demonstrated the ability of the inserted metal ions to undergo inner sphere oxidation with the reaction between NO and Fe-MOF-5. Iron nitrosyl complexes are widely studied due to their relevance to biology, and reactions involving nitric oxide are useful tests because the vibrational frequency of the N−O stretch offers insight into the electronic properties of the iron center. The reaction of NO gas with Fe-MOF-5 was monitored in situ by diffuse reflectance infrared Fourier transform spectroscopy (DRIFTS), as depicted in Figure 5. Upon exposure of activated Fe-MOF-5 to NO, a new resonance appears, centered at 1788 cm^{-1}. This is lower than the stretch (υ_{N-O}) of free NO (1876 cm^{-1}) and the υ_{N-O} we observed for pristine (all-zinc) MOF-5 after exposure to NO (1815 cm^{-1}) (see Figure S19 in the Supporting Information), indicating that NO is bound and activated at the iron center. PXRD of the resulting crystals confirms that they retain the MOF-5 crystalline lattice (see Figure S19 in the Supporting Information). The value of υ_{N-O} in Fe-MOF-5 is in fact lower than those observed in all other MOFs thus far (see

dx.doi.org/10.1021/ja4064475 | J. Am. Chem. Soc. 2013, 135, 12886−12891

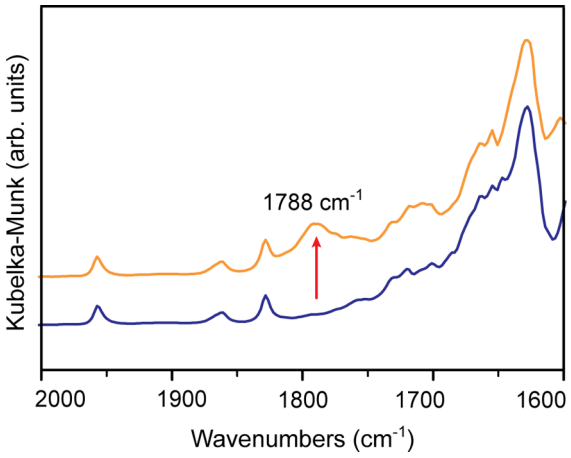

Figure 5. DRIFTS spectra of Fe-MOF-5 before (blue) and after (yellow) exposure to NO at room temperature and ambient pressure.

Table 2),[9,38−44] and is better compared to molecular species supported by similar ligand environments. Indeed, using the

Table 2. Comparison of υ_{N-O} and λ_{max} Values for the Nitrosyl-to-Iron Charge Transfer Band in (NO)Fe-MOF-5 with Relevant {Fe-NO}^{7} Complexes and Other MOFs

	υ_{N-O} (cm^{-1})	λ_{max} (nm)	system
HKUST-1	1887		MOF
Fe-ZSM-5	1880		zeolite
CPO-27-Ni	1843		MOF
MIL-100(V)	1841		MOF
MIL-100(Fe)	1825		MOF
MOF-5	1815		MOF
[Fe(nta)(NO)]	1793	342, 439	molecule
(NO)Fe-MOF-5	1788	395, 476	MOF
[Fe(1^{iPr})(NO)]	1739	350, 500	molecule
superoxide reductase	1721	475	enzyme
HemeA(NO)	1668		molecule
[Me_4N][Fe(NS_3)(NO)]	1639		molecule

Enemark and Feltham notation,[45] the MOF-5 ligand, abbreviated $O(O)_3^{2-}$ where O is the μ_4-oxo and O are the trigonally symmetric carboxylate arms of the $Zn_3O(O_2C-)_6^{2-}$ SBU, produces an {Fe-NO}^{7} complex that fits into a series of {Fe-NO}^{7} compounds based on trigonal tetradentate ligands denoted similarly as $N(O)_3^{3-}$,[46] $N(N)_3^{3-}$,[47] and $N(S)_3^{3-}$.[48] The greater electron density of $N(S)_3^{3-}$ in [Me_4N][Fe(NS_3)(NO)] and $N(N)_3^{3-}$ in [Fe(1^{iPr})(NO)] enhances the iron-to-NO backbonding, leading to lower values of υ_{N-O} (see Table 2). The $N(O)_3^{3-}$ scaffold in [Fe(nta)(NO)] would be expected to impart greater density on iron than MOF-5, though its υ_{N-O} is higher than that in (NO)FeMOF-5. This observation is in line with the assignment of O in MOF-5 as a strong Lewis base on the basis of EPR experiments (vide supra). Comparisons with other structurally unrelated ligand fields of biological {Fe-NO}^{7} species offer another basis for evaluating (NO)Fe-MOF-5. For instance, although both support pentacoordinate nitrosyl species, the biomolecule HemeA activates NO to a far greater degree than MOF-5 due to the strong ligand field of the porphyrin ring.[49] Conversely, the amino-acid ligand field of superoxide reductase generates only a slightly more activated nitrosyl species than MOF-5.[50] The zeolite Fe-ZSM-5, which is known to catalyze the reduction of NO by ammonia and thus binds NO, provides a relevant comparison with our material, but shows only weak NO binding with υ_{N-O} at 1880 cm^{-1}.[51]

(NO)Fe-MOF-5 also displays two new bands in the visible region of its electronic absorption spectrum, shown in Figure S20. The bands at 395 and 476 nm are characteristic of ligand-to-metal NO(π^*) → d charge transfer and are similar to transitions observed for the complexes in Table 2. Notably, returning the sample to vacuum reverts it to the original color, suggesting reversibility of the NO binding. EPR of (NO)Fe-MOF-5, shown in Figure S22, displays two signals at $g_{x,y}$ = 4.5 and g_z = 2.00. On the basis of assignments from similar {Fe-NO}^{7} complexes,[52] these reflect the axial symmetry of the ligand field and an overall $S = {}^3/_2$ arising from strong antiferromagnetic coupling between the $S = {}^5/_2$ iron and $S = {}^1/_2$ NO fragment. The corresponding transitions most likely result from $|\pm {}^1/_2\rangle$ states, whereas the splitting of $|\pm {}^3/_2\rangle$ is too large to observe under the experimental conditions. Hence, due to its heterogeneous nature, a {Fe-NO}^{7} fragment in the solid-state lattice of MOF-5 offers a distinct reactivity landscape from the solution-phase chemistry of metal nitrosyls and is the first such species in an *all-oxygen* ligand field. Unlike previous examples of NO activation by MOFs, the value of υ_{N-O} in (NO)Fe-MOF-5 is consistent with electron transfer by the metal center and portends novel redox transformations between the various MOF-5 analogues and small molecules, which we are currently investigating.

CONCLUSION

We have shown that redox-active di- and trivalent first row transition metals can be substituted into MOF-5 to give materials that are inaccessible by typical synthetic pathways. In particular, we have reported the first examples of Ti^{3+}- and V^{2+}-containing MOFs, along with five other previously unknown analogues of MOF-5 itself. The inserted metal ions resemble the molecular species of coordination chemistry and catalysis, yet the solid-state lattice provides a unique platform for future reactivity studies. As a proof of this concept, we demonstrated that outer-sphere electron transfer can be achieved in Cr-MOF-5 and that Fe-MOF-5 activates NO more than any other MOF. These experiments illustrate rare examples of stoichiometric redox reactivity at MOF SBUs and emphasize the unique coordination environment and ligand field character of the metal nodes when regarded as ligands.

ASSOCIATED CONTENT

Supporting Information

Synthetic and characterization procedures; computational details; EDX spectra of ClTi-MOF-5, ClCr-MOF-5, Mn-MOF-5, Fe-MOF-5; microscope images of (Cl)M-MOF-5; EPR spectra of ClTi-MOF-5, Mn-MOF-5, (NO)Fe-MOF-5, and ClCr-MOF-5; N_2 isotherms of (BF_4)Cr-MOF-5 and (Cl)M-MOF-5; DRIFTS of (NO)MOF-5; UV-vis-NIR spectra with TD-DFT transitions of ClTi-MOF-5, Cr-MOF-5, ClCr-MOF-5, (BF_4)Cr-MOF-5; UV−vis−NIR spectrum of (NO)Fe-MOF-5; optimized geometries of Cr-MOF-5 and ClCr-MOF-5. This material is available free of charge via the Internet at http://pubs.acs.org.

AUTHOR INFORMATION

Corresponding Author

mdinca@mit.edu

Notes

The authors declare no competing financial interest.

■ ACKNOWLEDGMENTS

This work was supported by the U.S. Department of Energy, Office of Science, Office of Basic Energy Sciences, under Award DE-SC0006937. We thank Thach Can for insightful conversations about simulating EPR spectra, Michael Huynh for assistance in collecting and interpreting scanning electron microscopy data, and the X-ray laboratory at the Department of Chemistry and Chemical Biology at Harvard University for providing the optical microscope and camera. C.K.B. gratefully acknowledges the NSF Graduate Research Fellowship Program for financial support through Grant 1122374.

■ REFERENCES

(1) Dincă, M.; Dailly, A.; Liu, Y.; Brown, C. M.; Neumann, D. A; Long, J. R. *J. Am. Chem. Soc.* **2006**, *128*, 16876−16883.
(2) Dhakshinamoorthy, A.; Alvaro, M.; Garcia, H. *Chem. Commun.* **2012**, *48*, 11275−11288.
(3) Phan, A.; Czaja, A. U.; Gándara, F.; Knobler, C. B.; Yaghi, O. M. *Inorg. Chem.* **2011**, *50*, 7388−7390.
(4) Bloch, E. D.; Murray, L. J.; Queen, W. L.; Chavan, S.; Maximoff, S. N.; Bigi, J. P.; Krishna, R.; Peterson, V. K.; Grandjean, F.; Long, G. J.; Smit, B.; Bordiga, S.; Brown, C. M.; Long, J. R. *J. Am. Chem. Soc.* **2011**, *133*, 14814−14822.
(5) Fu, Y.; Sun, D.; Chen, Y.; Huang, R.; Ding, Z.; Fu, X.; Li, Z. *Angew. Chem., Int. Ed.* **2012**, *51*, 3364−3367.
(6) Dan-Hardi, M.; Serre, C.; Frot, T.; Rozes, L.; Maurin, G.; Sanchez, C.; Férey, G. *J. Am. Chem. Soc.* **2009**, *131*, 10857−10859.
(7) The existence of Ti^{3+} has been observed during photoreduction studies with Ti^{4+}-containing MOFs: see refs 5 and 6.
(8) Murray, L. J.; Dincă, M.; Yano, J.; Chavan, S.; Bordiga, S.; Brown, C. M.; Long, J. R. *J. Am. Chem. Soc.* **2010**, *132*, 7856−7857.
(9) Wei, W.; Xia, Z.; Wei, Q.; Xie, G.; Chen, S.; Qiao, C.; Zhang, G.; Zhou, C. *Microporous Mesoporous Mater.* **2013**, *165*, 20−26.
(10) Ma, S.; Yuan, D.; Chang, J.-S.; Zhou, H.-C. *Inorg. Chem.* **2009**, *48*, 5398−5402.
(11) Halder, G. J.; Chapman, K. W.; Neville, S. M.; Moubaraki, B.; Murray, K. S.; Létard, J.-F.; Kepert, C. J. *J. Am. Chem. Soc.* **2008**, *130*, 17552−17562.
(12) Sumida, K.; Horike, S.; Kaye, S. S.; Herm, Z. R.; Queen, W. L.; Brown, C. M.; Grandjean, F.; Long, G. J.; Dailly, A.; Long, J. R. *Chem. Sci.* **2010**, *1*, 184−191.
(13) Brozek, C. K.; Dincă, M. *Chem. Sci.* **2012**, *3*, 2110−2113.
(14) Li, H.; Eddaoudi, M.; O'Keeffe, M.; Yaghi, O. *Nature* **1999**, *402*, 276−279.
(15) Das, S.; Kim, H.; Kim, K. *J. Am. Chem. Soc.* **2009**, *131*, 3814−3815.
(16) Song, X.; Kim, T. K.; Kim, H.; Kim, D.; Jeong, S.; Moon, H. R.; Lah, M. S. *Chem. Mater.* **2012**, *24*, 3065.
(17) Zhang, Z.; Zhang, L.; Wojtas, L.; Nugent, P.; Eddaoudi, M.; Zaworotko, M. J. *J. Am. Chem. Soc.* **2012**, *134*, 924−927.
(18) Zhang, Z.-J.; Shi, W.; Niu, Z.; Li, H.-H.; Zhao, B.; Cheng, P.; Liao, D.-Z.; Yan, S.-P. *Chem. Commun.* **2011**, *47*, 6425−6427.
(19) Prasad, T. K.; Hong, D. H.; Suh, M. P. *Chem.—Eur. J.* **2010**, *16*, 14043−14050.
(20) Kim, M.; Cahill, J. F.; Fei, H.; Prather, K. A.; Cohen, S. M. *J. Am. Chem. Soc.* **2012**, *134*, 18082−18088.
(21) Zhao, J.; Mi, L.; Hu, J.; Hou, H.; Fan, Y. *J. Am. Chem. Soc.* **2008**, *130*, 15222−15223.
(22) Huang, S.; Li, X.; Shi, X.; Hou, H.; Fan, Y. *J. Mater. Chem.* **2010**, *20*, 5695−5699.
(23) Denysenko, D.; Werner, T.; Grzywa, M.; Puls, A.; Hagen, V.; Eickerling, G.; Jelic, J.; Reuter, K.; Volkmer, D. *Chem. Commun.* **2012**, *48*, 1236−1238.
(24) Jacobs, T.; Clowes, R.; Cooper, A. I.; Hardie, M. J. *Angew. Chem., Int. Ed.* **2012**, *51*, 5192−5195.
(25) Wang, X.-J.; Li, P.-Z.; Liu, L.; Zhang, Q.; Borah, P.; Wong, J. D.; Chan, X. X.; Rakesh, G.; Li, Y.; Zhao, Y. *Chem. Commun.* **2012**, *48*, 10286−10288.
(26) Kim, Y.; Das, S.; Bhattacharya, S.; Hong, S.; Kim, M. G.; Yoon, M.; Natarajan, S.; Kim, K. *Chem.—Eur. J.* **2012**, *18*, 16642−16648.
(27) Lalonde, M.; Bury, W.; Karagiaridi, O.; Brown, Z.; Hupp, J. T.; Farha, O. K. *J. Mater. Chem. A* **2013**, *1*, 5453−5468.
(28) Although the existence of a supercell cannot be ruled out, the difficulty in using X-ray diffraction to determine this stems from the similar electron density for Zn and the inserted metal ions and the high symmetry of MOF-5.
(29) Irving, H.; Williams, R. J. P. *J. Chem. Soc.* **1953**, 3192.
(30) Botas, J. a.; Calleja, G.; Sánchez-Sánchez, M.; Orcajo, M. G. *Langmuir* **2010**, *26*, 5300−5303.
(31) Li, H.; Shi, W.; Zhao, K.; Li, H.; Bing, Y.; Cheng, P. *Inorg. Chem.* **2012**, *51*, 9200−9207.
(32) Definitive EDX spectra could not be obtained for Cr-MOF-5, ClV-MOF-5, and V-MOF-5 since the L edge of V and Cr nearly overlaps with the K edge of O. Detecting for Cr and V at the K edge by radiating at high energy destroyed the samples, making data collection impossible, yet sufficient data could be collected at the Cr K edge for ClCr-MOF-5 before compromising the crystal integrity.
(33) Drago, R. S. *Physical Methods for Chemists*, 2nd ed.; Saunders (W.B.) Co Ltd: Philadelphia, 1992; p 750.
(34) Ganesan, R.; Viswanathan, B. *J. Mol. Catal. A: Chem.* **2004**, *223*, 21−29.
(35) Ravikumar, R. V. S. S. N.; Komatsu, R.; Ikeda, K.; Chandrasekhar, A. V.; Reddy, B. J.; Reddy, Y. P.; Rao, P. S. *Solid State Commun.* **2003**, *126*, 251−253.
(36) Kaye, S. S.; Dailly, A.; Yaghi, O. M.; Long, J. R. *J. Am. Chem. Soc.* **2007**, *129*, 14176−14177.
(37) Walton, K. S.; Snurr, R. Q. *J. Am. Chem. Soc.* **2007**, *129*, 8552−8556.
(38) Xiao, B.; Wheatley, P. S.; Zhao, X.; Fletcher, A. J.; Fox, S.; Rossi, A. G.; Megson, I. L.; Bordiga, S.; Regli, L.; Thomas, K. M.; Morris, R. E. *J. Am. Chem. Soc.* **2007**, *129*, 1203−1209.
(39) Bonino, F.; Chavan, S.; Vitillo, J. G.; Groppo, E.; Agostini, G.; Lamberti, C.; Dietzel, P. D. C.; Prestipino, C.; Bordiga, S. *Chem. Mater.* **2008**, *20*, 4957−4968.
(40) McKinlay, A. C.; Xiao, B.; Wragg, D. S.; Wheatley, P. S.; Megson, I. L.; Morris, R. E. *J. Am. Chem. Soc.* **2008**, *130*, 10440−10444.
(41) Vimont, A.; Cortes, P. H.; Hwang, Y. K.; Ferey, G.; Daturi, M.; Chang, J.-S.; Serre, C.; Yoon, J. U.S. Patent 2012/0129684, May 24, 2010.
(42) We note that one other report of NO adsorption in a MOF recorded a new IR stretch at 1763 cm^{-1}, though this was likely assigned incorrectly as a Cu^{+}−NO species and may arise instead from the oxidation of Cu^{+} already in the structure: see the following two references.
(43) Wu, P.; Wang, J.; He, C.; Zhang, X.; Wang, Y.; Liu, T.; Duan, C. *Adv. Funct. Mater.* **2012**, *22*, 1698−1703.
(44) Szanyi, J.; Daturi, M.; Clet, G.; Baer, D. R.; Peden, C. H. F. *Phys. Chem. Chem. Phys.* **2012**, *14*, 4383−4390.
(45) Enemark, J.; Feltham, R. *Coord. Chem. Rev.* **1974**, *13*, 339−406.
(46) Schneppensieper, T.; Finkler, S.; Czap, A.; van Eldik, R.; Heus, M.; Nieuwenhuizen, P.; Wreesmann, C.; Abma, W. *Eur. J. Inorg. Chem.* **2001**, *2001*, 491−501.
(47) Ray, M.; Golombek, A. P.; Hendrich, M. P.; Yap, G. P. A.; Liable-Sands, L. M.; Rheingold, A. L.; Borovik, A. S. *Inorg. Chem.* **1999**, *38*, 3110−3115.
(48) Conradie, J.; Quarless, D. A; Hsu, H.-F.; Harrop, T. C.; Lippard, S. J.; Koch, S. A.; Ghosh, A. *J. Am. Chem. Soc.* **2007**, *129*, 10446−10456.
(49) Maxwell, J. C.; Caughey, W. S. *Biochemistry* **1976**, *15*, 388−396.
(50) Clay, M. D.; Cosper, C. A.; Jenney, F. E.; Adams, M. W. W.; Johnson, M. K. *Proc. Natl. Acad. Sci. U.S.A.* **2003**, *100*, 3796−3801.

(51) Long, R. Q.; Yang, R. T. *J. Am. Chem. Soc.* **1999**, *121*, 5595−5596.
(52) Lee, M.; Arosio, P.; Cozzi, A.; Chasteen, N. D. *Biochemistry* **1994**, *33*, 3679−3687.